Molecular Environment and Temperature Dependence of Hyperfine Interactions in Sugar Crystal Radicals from First Principles

R. Declerck, E. Pauwels, V. Van Speybroeck, and M. Waroquier*

Center for Molecular Modeling, Ghent University, Proeftuinstraat 86, B-9000 Gent, Belgium

Received: August 15, 2007; In Final Form: October 16, 2007

The effect of the molecular environment and the temperature dependence of hyperfine parameters in first principles calculations in α-D-glucose and β-D-fructose crystal radicals have been investigated. More specifically, we show how static (0 K) cluster in vacuo hyperfine calculations, commonly used today, deviate from more advanced molecular dynamics calculations at the experimental temperature using periodic boundary conditions. From the latter approach, more useful information can be extracted, allowing us to ascertain the validity of proposed molecular models.

1. Introduction

Over the past few decades, radiation-induced radicals in solid-state sugars have received considerable attention.[1−3] These carbohydrates are extremely abundant in plants and animals and play an essential role in several biological processes. A prominent technique to detect such radical defects is electron paramagnetic resonance (EPR) spectroscopy. In recent years, there has been a growing interest in the ab initio quantum mechanical calculation of these EPR quantities within density functional theory (DFT).[4,5] A comprehensive overview is given in ref 6. By comparing the experimental EPR quantities with those computed from proposed molecular models, it is possible to identify and understand the microscopic structure of these defects.

The energy levels and intensities derived from EPR experiments can be reproduced using an effective Hamiltonian which, in the case of these radicals, involves three principal quantities: (i) the hyperfine parameters (HFPs), (ii) the **g** tensor, and (iii) the zero-field splitting tensor. In this paper, we will focus on the first quantity. The HFPs can be computed from the ground state spin density alone, and they probe the spin density of a region near the nucleus.

A recurring problem in the calculation of theoretical HFPs (see, for example, refs 7−9) concerns the inclusion of the molecular environment (ME) in these sugar crystal radicals. One of the most commonly used ME models is the cluster in vacuo approach. Conceptually, this approach is based on the assumption that the embedding of the radical molecule in a sufficiently large cluster mimics the electronic confinement of the radical in the crystalline lattice: a central radical structure is surrounded by molecules fixed in space at the geometry of the crystal structure, and the HFPs can then be readily calculated using the available gas-phase methods.

However, a more natural and more accurate way to simulate crystalline lattices is to perform periodic boundary calculations, thereby exploiting the translational symmetry of the crystalline state. The first purpose of this work is to assess the accuracy of HFPs calculated using different cluster in vacuo approximations found in the literature by comparing them with a reference set of HFPs calculated from periodic boundary simulations. Several methods have been described in the literature to calculate HFPs from such simulations.[10−14] In this work, we will make use of the efficient hybrid HFP scheme recently proposed by the authors in ref 15 and reiterated here briefly in the next section.

Previous HFP calculations by the authors on these sugar crystal radicals were all static (at 0 K) and did not account for the effects that may occur at the finite experimental temperature. The second purpose of this work is to investigate, using the hybrid HFP scheme, the effects of temperature on the HFPs by averaging the HFPs calculated at every step along a Born−Oppenheimer molecular dynamics trajectory equilibrated at the experimental temperature. Some similar work has been done in the past, such as the investigation of temperature effects on nuclear magnetic resonance chemical shifts[16,17] and nuclear quadrupole coupling constants.[18]

2. Theory and Computational Details

The components of the hyperfine tensor $\mathbf{A}_N$ of a nucleus N can be derived from relativistic many-body quantum mechanics, and the most dominant terms are[19,20]

$$A_{N,ij} = A_{\mathrm{iso},N}\delta_{ij} + A_{\mathrm{ani},N,ij} \tag{1}$$

where

$$A_{\mathrm{iso},N} = \frac{1}{3}\frac{g_e\mu_e g_N\mu_N}{\langle S_z\rangle}\int \mathrm{d}\mathbf{r}\ \rho_s(\mathbf{r})\delta_T(\mathbf{r}) \tag{2}$$

$$A_{\mathrm{ani},N,ij} = \frac{1}{8\pi}\frac{g_e\mu_e g_N\mu_N}{\langle S_z\rangle}\int \mathrm{d}\mathbf{r}\ \rho_s(\mathbf{r})\frac{3r_ir_j - \delta_{ij}r^2}{r^5} \tag{3}$$

Here, $\rho_s = \rho^\alpha - \rho^\beta$ represents the net electronic spin density, g_e is the free-electron g value, μ_e is the Bohr magneton, g_N is the nuclear gyromagnetic ratio for the nucleus, μ_N is the nuclear magneton, $\langle S_z\rangle$ is the expectation value of the z-component of the total electronic spin, and the vector $\mathbf{r}$ is taken relative to the position of the nucleus. The isotropic HFP A_{iso} corresponds to the Fermi contact interaction, whereas the anisotropic HFPs $A_{\mathrm{ani},ij}$ results from dipole−dipole interactions. $\delta_T(\mathbf{r})$ is a smeared out δ function that results from scalar relativistic corrections.[10,19] The subscripts i and j refer to Cartesian coordinates x, y, and z. The gyromagnetic ratio data used in this paper originate from ref 21.

10.1021/jp076571w CCC: $40.75
Published on Web 01/12/2008

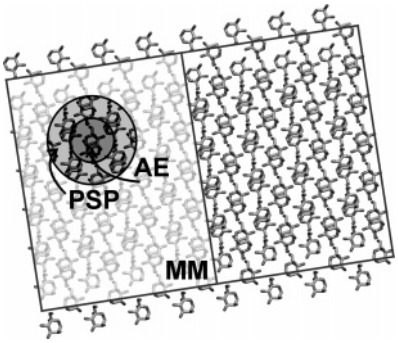

Figure 1. Sketch of the hybrid AE + PSP GAPW scheme, extended with a third MM layer. The simulation cell and one of its neighboring images are shown.

In ref 15, we introduced a method for the calculation of hyperfine parameters in extended systems under periodic boundary conditions using the Gaussian and augmented-plane-wave (GAPW) density functional method. The HFP method was implemented in the Quickstep[22] code, which is part of the freely available program package CP2K.[23] In the GAPW method, the total density is described in a smooth, extended part represented in plane waves and parts localized close to the nuclei that are expanded in periodic Gaussian functions. The GAPW method exists in both a pseudopotential (PSP)[24] and an all-electron (AE)[25] implementation, and both approaches can be easily combined within one simulation. Using a supercell technique to approximate the gas phase, we have shown for a variety of atomic and molecular species that the AE GAPW method reproduces the HFPs calculated from pure gas-phase calculations to within less than 2%. We have also introduced an efficient hybrid HFP calculation scheme, in which an AE treatment for the nuclei of interest and a PSP approximation for the remaining atoms in the simulation cell are combined. It has been shown that the use of this hybrid AE + PSP GAPW scheme does not significantly alter the results obtained with an AE treatment for the entire simulation cell and, hence, makes HFP predictions in large systems computationally more affordable. The scheme could even be extended easily to a three-layer scheme including a classical molecular mechanics (MM) layer, as sketched in Figure 1, allowing for the study of HFPs in even larger molecular systems.

The HFP calculations within the different cluster in vacuo approximations were performed using the Gaussian 03[26] program package. However, whenever possible, they were independently corroborated with the Quickstep HFP code using the aforementioned supercell technique.

3. Effect of the Molecular Environment

Since the hybrid AE + PSP GAPW scheme allows the calculation of HFPs in extended systems under periodic boundary conditions with the AE accuracy that for long has been accessible only to simple gas-phase systems, it can be used as a reference method to evaluate different cluster in vacuo methods for HFP calculations described in the literature. In this comparison, we will consider low-temperature (77 K) radiation-induced radical structures in α-D-glucose and β-D-fructose (see Figure 2), further referred to as Gluc/R1, Gluc/R2, Fruc/R1, and Fruc/R2. These radical structures were proposed in earlier publications.[9,29,30]

It was derived from neutron diffraction studies[31,32] that both the α-D-glucose and the β-D-fructose crystals are orthorhombic, with the former featuring unit cell constants of $a = 19.59$ au, $b = 28.06$ au, and $c = 9.40$ au and the latter, unit cell constants

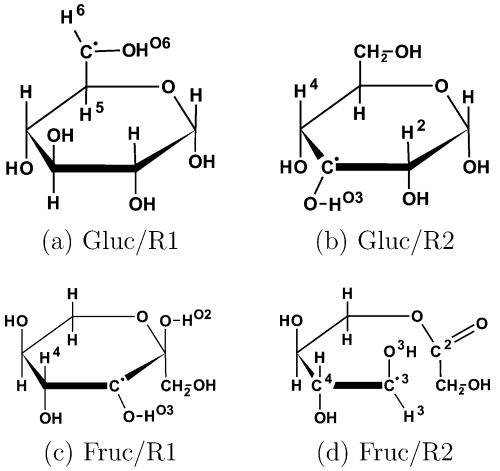

Figure 2. Radical structures in α-D-glucose (a and b) and β-D-fructose (c and d). Some atoms are labeled in superscript for further reference.

of $a = 17.37$ au, $b = 18.98$ au, and $c = 15.30$ au. In the periodic boundary simulations, we doubled the unit cell in the c direction for α-D-glucose (denoted as ab2c) and in the a and c directions for β-D-fructose (2ab2c) to ensure that radicals from neighboring periodic images remain well-separated from each other. The cluster in vacuo models comprised all molecules that are engaged in hydrogen bonds with the central radical in accordance with the crystal structure. This choice for the cluster size corresponds to earlier work, in which it was argued that the intermolecular interactions in crystalline sugars are predominantly governed by hydrogen bonds. Geometry optimizations were performed on the central radical while keeping the coordinates of the surrounding molecules fixed in space at the geometry of the crystal structure.

For a reliable assessment, all calculation details not related to the different ME models have been kept as uniform as possible. A BLYP gradient-corrected exchange-correlation (XC) functional[33,34] was used throughout all calculations. In the periodic boundary model, we used a TZVP-AE[35] basis set and an AE description for the radical and a TZVP-PSP[36] basis set and pseudopotentials of Goedecker and co-workers[37,38] for the undamaged molecules in the simulation cell. Geometry relaxations using this scheme showed that Gluc/R1 was more stable than Gluc/R2 by 3.3 au (8.7 kJ/mol), whereas Fruc/R1 was more stable than Fruc/R2 by 8.0 au (21.0 kJ/mol). In the cluster in vacuo models, the TZVP-AE basis set was consistently employed for the central radical, and the surrounding molecules were treated using various techniques: (i) at the same level of theory as the central radical (full cluster), (ii) at the semiempirical PM3[39,40] level using an Oniom[41−45] technique (Oniom cluster), or (iii) not including the molecular environment at all (radical molecule).

In Table 1, the calculated HFPs are classified according to the ME model (periodic, full cluster, Oniom cluster, or radical molecule) used for relaxing the geometry as well as for the subsequent HFP calculation. As can be observed, the applied ME models can be different for the two steps in the simulation because of the fact that the geometry relaxation often poses a much larger computational burden. The first set of HFPs (denoted as periodic/periodic) were calculated using the reference hybrid AE + PSP GAPW scheme. The other sets of theoretical HFPs are arranged according to the decreasing size of the ME models. The values between brackets denote the angles (in degrees) of the principal directions with respect to the corresponding reference principal directions. The experimental HFPs (and their angular deviations with respect to the

TABLE 1: Proton ^{1}H HFPs (in MHz) for the Gluc/R1 and Gluc/R2 Radicals in α-D-Glucose, and the Fruc/R1 and Fruc/R2 Radicals in β-D-Fructose, Using Various Periodic and Cluster in Vacuo Methods, Classified Both by the ME Model Used to Relax the Geometry and by the Model Used for the Subsequent HFP Calculation Based on This Relaxed Geometry[a]

geometry relaxation HFP calculation		periodic[b] periodic[b]				periodic[b] full cluster[c]				full cluster[c] full cluster[c]			
		A_{iso}	$A_{ani,xx}$	$A_{ani,yy}$	$A_{ani,zz}$	A_{iso}	$A_{ani,xx}$	$A_{ani,yy}$	$A_{ani,zz}$	A_{iso}	$A_{ani,xx}$	$A_{ani,yy}$	$A_{ani,zz}$
						α-D-Glucose							
Gluc/R1	H6	−49.9	−33.4	−1.6	35.0	−49.7	−33.3 (0.3°)	−1.4 (0.0°)	34.7 (0.8°)	−50.9	−33.7 (3.8°)	−1.0 (6.5°)	34.7 (5.4°)
	H5	26.9	−6.3	−3.2	9.4	26.4	−6.2 (1.4°)	−3.2 (1.0°)	9.4 (0.7°)	37.0	−6.2 (3.6°)	−3.0 (3.4°)	9.2 (2.4°)
	HO6	6.4	−11.2	−8.3	19.5	6.1	−11.3 (1.6°)	−8.6 (1.5°)	19.9 (0.0°)	3.9	−11.5 (15.4°)	−8.8 (15.4°)	20.2 (0.7°)
Gluc/R2	H2	95.4	−5.0	−1.4	6.5	90.5	−4.8 (6.3°)	−2.0 (6.6°)	6.8 (2.1°)	93.0	−4.6 (11.2°)	−2.1 (11.3°)	6.6 (1.3°)
	H4	87.3	−5.1	−2.0	7.1	84.9	−4.9 (1.9°)	−2.4 (2.7°)	7.3 (2.1°)	88.2	−4.8 (5.4°)	−2.5 (5.5°)	7.3 (2.0°)
	HO3	6.6	−10.8	−8.5	19.3	6.6	−11.0 (1.1°)	−8.9 (1.0°)	19.9 (0.8°)	1.9	−11.4 (3.3°)	−8.7 (2.2°)	20.1 (3.0°)
						β-D-Fructose							
Fruc/R1	H4	98.9	−5.2	−1.6	6.8	99.9	−5.1 (1.2°)	−1.7 (1.1°)	6.8 (0.0°)	98.6	−5.1 (0.9°)	−1.7 (1.8°)	6.9 (1.5°)
	HO2	17.9	−3.8	−1.9	5.7	18.2	−3.5 (4.4°)	−2.1 (4.4°)	5.5 (0.4°)	19.1	−3.5 (3.1°)	−2.1 (2.7°)	5.5 (1.5°)
	HO3	8.8	−11.3	−8.8	20.0	8.9	−11.2 (4.3°)	−8.9 (4.4°)	20.1 (0.3°)	8.7	−11.2 (7.8°)	−8.9 (7.8°)	20.1 (1.9°)
Fruc/R2	H3	−27.4	−30.4	−1.5	31.9	−28.5	−30.7 (0.4°)	−1.5 (0.7°)	32.2 (0.8°)	−46.8	−34.1 (4.5°)	−1.0 (4.8°)	35.2 (2.5°)

geometry relaxation HFP calculation		oniom cluster[d] full cluster[c]				oniom cluster[d] radical molecule[c]				experiment[e]			
		A_{iso}	$A_{ani,xx}$	$A_{ani,yy}$	$A_{ani,zz}$	A_{iso}	$A_{ani,xx}$	$A_{ani,yy}$	$A_{ani,zz}$	A_{iso}	$A_{ani,xx}$	$A_{ani,yy}$	$A_{ani,zz}$
						α-D-Glucose							
Gluc/R1	H6	−37.0	−32.2 (3.8°)	−2.3 (13.3°)	34.5 (12.9°)	−30.5	−32.1 (4.1°)	−2.1 (11.1°)	34.3 (10.4°)	±57.8	±34.8 (1.2°)	∓2.2 (5.4°)	∓31.4 (5.5°)
	H5	13.2	−6.2 (5.1°)	−3.6 (5.0°)	9.8 (2.0°)	14.0	−6.1 (5.9°)	−3.7 (5.7°)	9.7 (2.1°)	19.3	−5.7 (24.0°)	−4.2 (23.5°)	10.0 (2.5°)
	HO6	−9.5	−12.7 (18.6°)	−7.7 (30.2°)	20.4 (27.0°)	−11.5	−13.8 (15.3°)	−8.5 (29.0°)	22.2 (27.6°)	±9.0			
Gluc/R2	H2	95.1	−4.6 (9.1°)	−2.1 (9.4°)	6.7 (5.1°)	87.2	−4.5 (10.4°)	−1.9 (11.0°)	6.5 (5.2°)	95.3	−4.8 (7.8°)	−2.0 (9.3°)	6.7 (4.9°)
	H4	87.2	−4.9 (2.1°)	−2.4 (2.6°)	7.2 (2.4°)	82.6	−4.8 (7.4°)	−2.4 (8.7°)	7.2 (4.9°)	89.4	−5.1 (9.6°)	−1.6 (9.6°)	7.1 (6.2°)
	HO3	1.5	−11.1 (13.1°)	−8.9 (11.3°)	20.0 (8.1°)	1.6	−11.7 (8.6°)	−8.8 (5.6°)	20.5 (8.9°)	5.6/28.0			
						β-D-Fructose							
Fruc/R1	H4	102.3	−5.2 (1.7°)	−1.8 (1.6°)	6.9 (1.1°)	97.1	−4.9 (7.6°)	−2.4 (8.8°)	7.3 (4.4°)	99.41	−5.01 (2.0°)	−1.99 (3.8°)	7.00 (3.4°)
										98.58	−5.08 (5.5°)	−1.87 (6.9°)	6.95 (4.3°)
	HO2	14.8	−3.8 (17.7°)	−1.9 (16.7°)	5.7 (6.8°)	19.9	−3.4 (18.8°)	−1.8 (18.7°)	5.2 (6.7°)	17.63	−3.57 (1.7°)	−2.29 (1.8°)	5.86 (0.7°)
	HO3	12.8	−11.0 (16.2°)	−9.2 (16.3°)	20.2 (3.0°)	14.4	−11.3 (5.7°)	−9.1 (6.6°)	20.4 (4.5°)				
Fruc/R2	H3	−46.8	−33.4 (5.7°)	−1.0 (6.8°)	34.4 (3.9°)	−45.3	−32.5 (5.8°)	−1.3 (6.7°)	33.8 (3.7°)	−45.59	−34.60 (2.1°)	1.66 (1.6°)	32.94 (1.7°)
										−38.88	−32.65 (5.4°)	3.63 (7.1°)	29.03 (7.7°)

[a] The values in parentheses denote the angles (in degrees) of the principal directions with the corresponding reference hybrid AE + PSP GAPW principal directions. The experimental HFPs are also given. [b] GAPW AE+PSP BLYP/TZVP/200Ry. [c] G03 AE BLYP/TZVP. [d] G03/ONIOM AE+PM3 BLYP/TZVP. [e] Experimental data from refs 27 and 28 (Gluc/R1 and Gluc/R2) and ref 29 (Fruc/R1 and Fruc/R2).

reference results) are also given; in some cases, no unique experimental signal could be attributed to the theoretical HFP prediction. Only the couplings for which experimental values from literature were available are taken up in Table 1. These couplings all involve protons, as they are generally more affordable to detect in EPR experiments than carbons or oxygens. Even when looking only at protons, an all-electron treatment is required, because the hydrogen PSP has a non-Coulombic shape near the core site, which affects the electronic spin density there and, hence, the corresponding HFPs, and thus, even in the simple case of protons, a HFP reconstruction procedure such as the one proposed in ref 46 would be necessary to correct for this deficiency. A HFP calculation using only PSPs on the optimized geometry of (for example) Gluc/R2 illustrates this: the isotropic HFPs of Gluc/R2/H2, Gluc/R2/H4, and Gluc/R2/HO3 become 78.9, 72.3, and 5.7 MHz. The ^{13}C HFPs of the C3 carbon in the radical center of Fruc/R2 (denoted as Fruc/R2/C3) will be discussed later on, even though no experimental

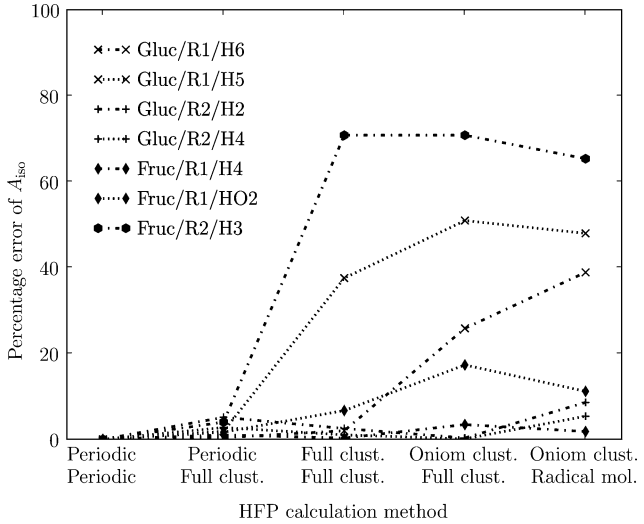

Figure 3. Percentage error of a selection[47] of isotropic HFPs with respect to the reference hybrid AE + PSP GAPW calculations for different cluster in vacuo methods (for notation, see Table 1).

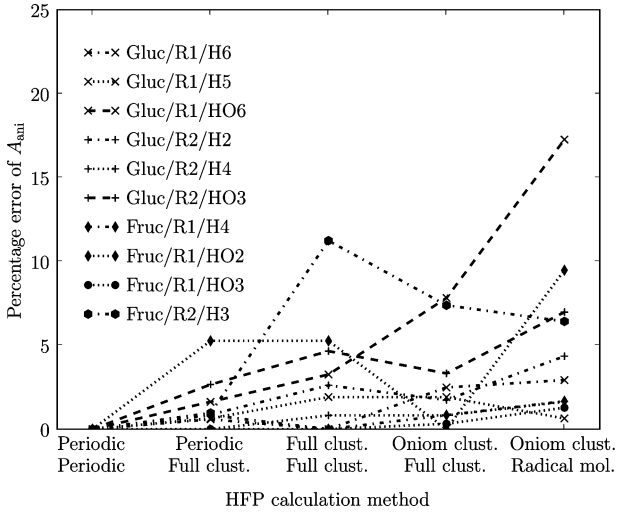

Figure 4. Percentage error of the anisotropy with respect to the reference hybrid AE + PSP GAPW calculations for different cluster in vacuo methods (for notation, see Table 1).

TABLE 2: Carbon ^{13}C HFPs (in MHz) for Fruc/R2/C3, Using Various Periodic and Cluster in Vacuo Methods[a]

type	A_{iso}	$A_{ani,xx}$	$A_{ani,yy}$	$A_{ani,zz}$
periodic/periodic	89.7	−65.2	−64.2	129.4
periodic/full cluster	92.2	−66.1 (1.0°)	−65.1 (1.0°)	131.2 (0.0°)
full cluster/full cluster	79.5	−73.4 (7.8°)	−72.1 (6.5°)	145.5 (4.3°)
Oniom cluster/full cluster	76.1	−70.7 (39.8°)	−71.9 (24.4°)	142.6 (34.4°)
Oniom cluster/radical molecule	74.3	−69.1 (41.6°)	−70.0 (27.6°)	139.0 (34.4°)

[a] For notation, see Table 1. The values between brackets denote the angles (in degrees) of the principal directions with the corresponding reference hybrid AE + PSP GAPW principal directions.

data is available for this coupling. The full list of calculated HFPs is available as Supporting Information.

Inspection of Table 1 shows that the agreement with the reference hybrid AE + PSP GAPW calculations diminishes when a less accurate description of the ME is employed. This effect is particularly pronounced for the isotropic HFPs: in Gluc/R1/H6, Gluc/R1/H5, Gluc/R1/HO6, and Fruc/R2/H3, these couplings can fluctuate by up to around 20 MHz from their reference value. The percentage errors for a selection[47] of isotropic HFPs with the reference calculations are shown in Figure 3 to illustrate the relative degradation of each particular isotropic HFP. From this figure, it becomes clear that the periodic/full cluster and the reference HFPs differ only marginally. The same accounts for the Oniom cluster/full cluster and the Oniom cluster/radical molecule combinations, especially when taking into account the oversimplification of the model in the evaluation of the HFPs, retaining only the radical in the complete absence of its molecular environment. Apparently, the ME model used in the geometry relaxation is the determining factor in the reproduction of the isotropic HFPs.

In the case of the isotropic HFP of Fruc/R2/H3, all methods featuring a cluster geometry relaxation deviate some 20 MHz from their reference value, and surprisingly, enough reproduce almost exactly one of the corresponding experimental values. The origin of this phenomenon can be attributed to the size of the cluster used for the geometry relaxation of the radical. The hydrogen-bonded undamaged molecules do not adequately embed the central radical and fail to impose the constraints imposed by the lattice structure. As a result, the disrupted bond in the radical is overestimated by 0.51 au (full cluster) and by 0.55 au (Oniom cluster) with respect to the periodic prediction of 4.77 au. The enlargement of the disrupted bond causes the electronic configuration in the C3 carbon of Fruc/R2 (for notation, see Figure 2d) to shift from sp to sp hybridization, the unpaired electron becomes more localized on this C3 carbon and influences the HFPs of the radical center due to their dependence on the spin density (eq 2). Similar effects were reported previously by Barone et al.[48−50] A comparison of the different C3 carbon HFP predictions in Table 2 supports this proposition: there exists a quite distinct difference between the HFPs that were obtained using a periodic geometry and those using a cluster geometry. Table 2 even reveals the dissimilarity between full cluster and Oniom cluster geometry HFP predictions. By doubling the number of neighbors in the cluster (from 8 to 16), the shortcomings of the cluster model disappear: after geometry relaxation of the central radical in the enlarged cluster model, its geometry matches perfectly with the periodic geometry. For example, the disrupted bond agrees to within <0.002 au. The isotropic HFPs for Fruc/R2/H3 and Fruc/R2/C3 become −31.5 and 95.6 MHz, respectively, which is in both cases closer to the corresponding periodic/periodic values. Hence, this proves that the initial good agreement with experimental results was only coincidental and that the actual deviation, obtained with an accurate incorporation of the ME, amounts to 11.5−18.2 MHz.

The changes in the anisotropic HFPs are more subtle. These fluctuations can be quantified by the anisotropy A_{ani}, defined as the difference between the maximum and the minimum anisotropic HFPs. Throughout Table 1, the disagreement with the reference data did not exceed 7 MHz. The percentage errors of the anisotropy with respect to the reference hybrid AE + PSP GAPW calculations are plotted in Figure 4. They remain lower than 20%, affirming the less pronounced sensitivity of A_{ani} on the ME description. Their corresponding principal directions vary a bit more and can deviate up to around 30° from the reference calculations. The arithmetic means of the angular deviations of each hyperfine coupling are plotted in Figure 5.

In conclusion, the cluster in vacuo methods used here were all able to reproduce the reference HFPs reasonably well. The largest fluctuations were found in the isotropic HFPs. In a few cases, the cluster size was found to be too small to closely

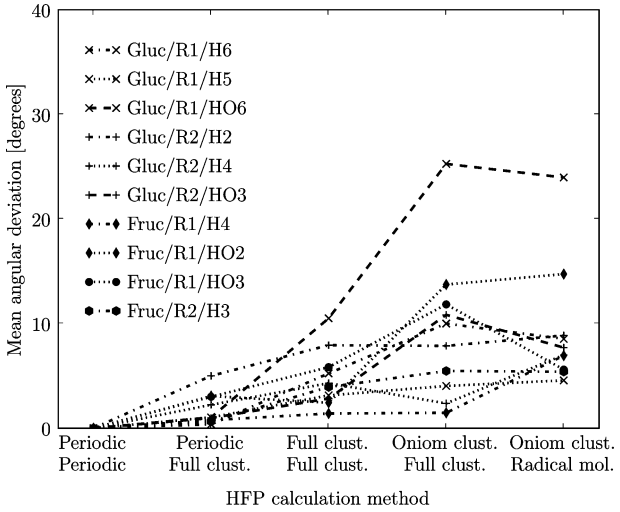

Figure 5. Mean angular deviation of the principal directions from the reference hybrid AE + PSP GAPW calculations for different cluster in vacuo methods (for notation, see Table 1).

reproduce the reference isotropic HFPs. All methods resulted in a good qualitative agreement with experimental data.

4. Effect of the Finite Temperature

The experimental HFPs from Table 1 were all obtained at the experimental temperature of 77 K. Thermally induced vibrations that involve inversion at the radical center are known to affect the HFPs.[48] This can occur due to shifts in the average bond lengths, bond angles, or dihedral angles from their static (0 K) value, which result from anharmonicities in their respective potentials, or are due to nonlinear dependencies that may exist between the HFPs and these geometric parameters. To include these temperature effects in HFP predictions, HFPs were calculated at every step along a Born−Oppenheimer molecular dynamics trajectory equilibrated at the experimental temperature and were subsequently averaged. These calculations were performed on the Fruc/R2 radical, because they may help to unravel the remaining discrepancy between the experimental and the static theoretical isotropic HFPs of Fruc/R2/H3 (see the discussion in the previous section).

Although the hybrid AE + PSP GAPW scheme heavily facilitates the instantaneous evalution of the HFPs, the Fruc/R2/H3 radical was simulated using only the unit cell (abc) as the simulation cell in order to further alleviate the computational burden. The system was sampled at the experimental temperature of 77 K using chains of Nosé−Hoover thermostats[51] attached to the nuclear degrees of freedom. After equilibration of the structure for 1.0 ps, its HFPs were computed on the fly during a production run of another 3.0 ps of canonical MD.

In Figure 6, the time evolution of the Fruc/R2/H3 isotropic HFP is plotted, together with some determining geometrical parameters of the radical center. As apparent, the isotropic coupling varies considerably, from 0 to −52 MHz, and comprises both reported experimental values. Averaging these values (see Table 3) results in an isotropic HFP which is a mere 1.7 MHz closer to the experimental values than the static (0 K) value obtained using the same (abc) simulation cell. Note that the latter result slightly differs from the result reported in Table 1 because of the use of a smaller simulation cell, resulting in a higher interaction with neighboring radicals: the radical from the smaller simulation cell is 4.4 au (11.4 kJ/mol) less stable than the radical from the larger (2ab2c) simulation cell and has geometric features, such as a lower improper dihedral C4−O3−H3−C3 (by 0.3°), that can be related to the Fruc/R2/H3 isotropic HFP prediction (see below). The cumulative averages of the isotropic HFPs at every 100 fs are also taken up in Figure 6 and illustrate the well-converged behavior of this value. The set of anisotropic HFPs and their principal directions comprise both experimental values, as well, but their averages are essentially not different from the static (0 K) values, and the averaged principal directions retain the excellent agreement with

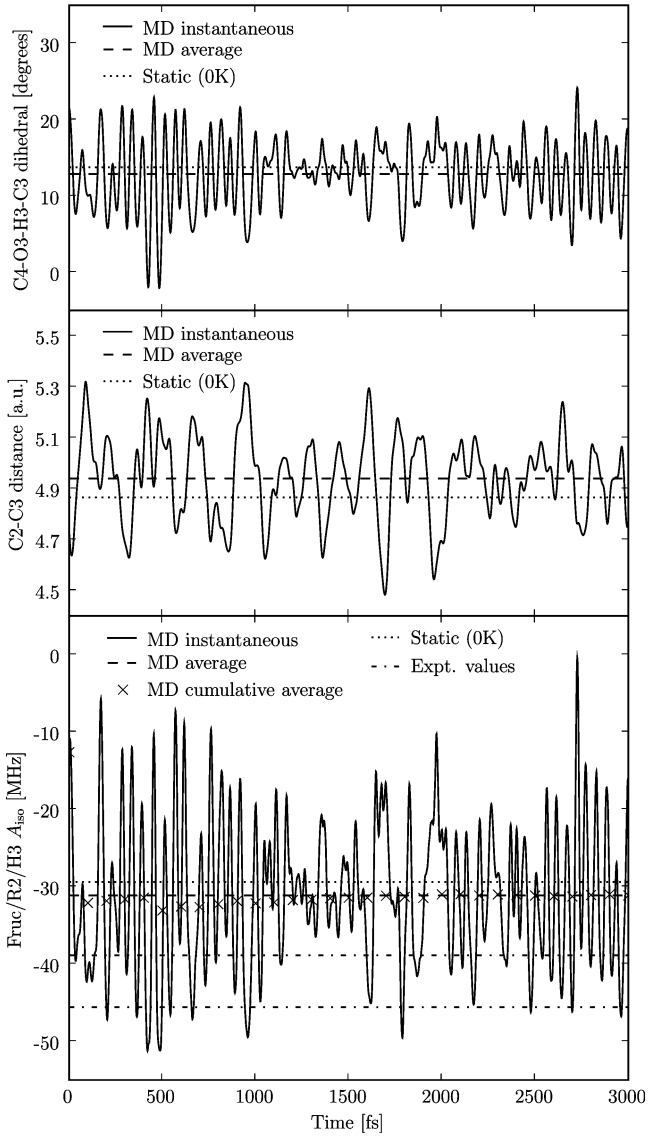

Figure 6. C4−O3−H3−C3 dihedral angle, C2−C3 bond length, and isotropic HFP for Fruc/R2/H3, calculated at every step of a 3 ps MD run (MD instantaneous). The average from all time steps (MD average), the static (0 K) value, and (in the case of the isotropic HFP) the cumulative average at every 100 fs (MD cumulative average) and both experimental values are also shown.

TABLE 3: Proton ^{1}H HFPs (in MHz) for Fruc/R2/H3, Averaged from HFP Calculations at Every Step in the MD or Calculated from the Static Geometry (at 0 K)[a]

type	A_{iso}	$A_{ani,xx}$	$A_{ani,yy}$	$A_{ani,zz}$
77 K	−31.1	−30.5 (1.4°)	−0.8 (1.5°)	31.6 (3.0°)
0 K	−29.4	−30.5 (1.7°)	−1.5 (2.1°)	32.0 (2.5°)
exptl	−45.59	−34.6	1.7	33.0

[a] The values in parentheses denote the angles (in degrees) of the principal directions with the corresponding principal directions of one of the experimental couplings (taken from Table 1).

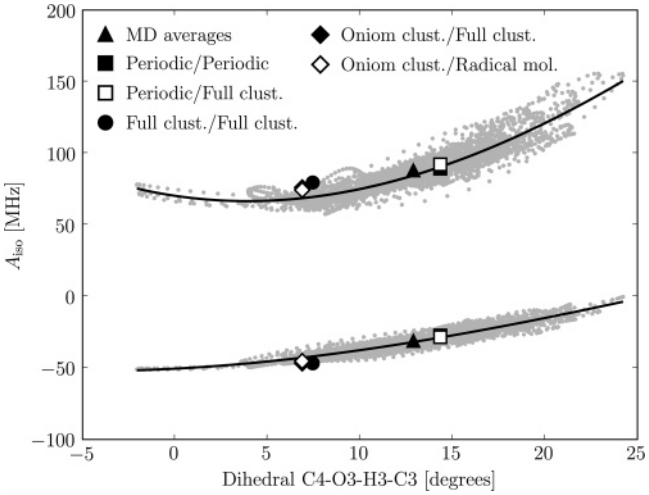

Figure 7. Correlation of the isotropic HFPs of both Fruc/R2/H3 and Fruc/R2/C3 and the C4−O3−H3−C3 dihedral angle. The solid lines represent a best fit of a third-order polynomial to the respective data sets, and the triangle symbols show the intersection point of the averaged values on the *x*- and *y*-axes. For the purpose of reference, results from static HFP calculation methods have also been included (for notation, see Table 1).

one of the experimental couplings. Thus, in this case, temperature effects account for only some, but far from all, of the discrepancies between the theoretical and experimental HFPs of Fruc/R2/H3.

To determine the origin of the large fluctuations in the isotropic HFP of Fruc/R2/H3, it is instructive to derive from the MD simulation some characteristic geometric features that may influence A_{iso}. Two relevant geometric parameters are the C2−C3 broken bond distance and the improper dihedral C4−O3−H3−C3, which represents a measure for the planarity of the radical center (for notation, see Figure 2d). Together, they reflect the continuous variation in the simulation of the electronic configuration in the C3 carbon of Fruc/R2 from sp^3 to sp^2 hybridization. Both parameters are plotted in Figure 6 along the MD trajectory. Averaging these parameters over the simulation period results in small but significant changes: the separation between C2 and C3 is enlarged by 0.1 au, and the radical center becomes more planar by 0.9°. Hence, the potential energy is asymmetric with respect to the planarity and tends to favor a more planar radical center. This is important, because the planarity of a radical center is known to have a significant influence on the isotropic HFP of α-protons, such as Fruc/R2/H3.[52] Figure 7 shows that there is a strong correlation between the isotropic HFP of Fruc/R2/H3 and the planarity. This feature is also present for the Fruc/R2/C3 isotropic HFP, which was also evaluated along the MD trajectory. The plots in Figure 7 clearly reveal the nonlinear dependency of both isotropic HFPs with respect to the planarity. As the radical center switches from sp^3 to sp^2 hybridization in the temperature simulation, the Fruc/R2/H3 isotropic HFP covers a wide range of over 50 MHz. This actually has the same effect as the mechanism causing the discrepancy between the cluster and periodic isotropic HFPs for Fruc/R2/H3 (see the previous section): the unpaired electron density on the C3 carbon fluctuates and influences the HFPs near the radical center due to their dependence on the spin density. Here, the added value of the MD simulation becomes clearly visible: the strong relationship between the planarity and the HFPs of Fruc/R2/H3 shows that the discrepancies between the theoretical and experimental HFPs of Fruc/R2/H3 are due to rather minor geometrical changes, thus, to some degree strengthening the validity of the theoretical model for the Fruc/R2 radical. Similar dependencies were derived earlier in theoretical studies of a glycine radical[48] and the methyl radical,[53] but employing a perturbational approach to account for finite temperature effects on the HFPs.

However, the MD simulation does not reveal the real origin of the observed discrepancies; neither does it explain the occurrence of two alike HFPs in the experimental spectra. In fact, it does not even rule out completely the existence of another structure representing the actual radical. Several factors other than temperature may play an important role. The use of a different XC functional, the PBE[54] functional, in both the geometry relaxation and the HFP calculation gave rise to a shift in the isotropic HFP of Fruc/R2/H3 of a mere 1.6 MHz, but in the opposite direction of both experimental values. Averaging over the zero-point motion[55,56] of the Fruc/R2/H3 proton will also affect the HFP predictions. The incorporation of the quantum nature of the nuclei can be included by performing path integral molecular-dynamics simulations,[57] which have not been considered here. There are also some known issues with DFT-based MD simulations,[58] such as nonergodic behavior at lower temperatures; however, the problems discussed in ref 58 primarily relate to condensed aqueous systems. One phenomenon that could deal with the two aforementioned problems at once involves the occurrence of proton transfer along the infinite hydrogen bond chains pervading throughout the entire crystal. The existence of stable structures featuring different types of proton transfer may alter the geometrical parameters that influence the HFPs of Fruc/R2/H3 in a different way; hence, resulting in multiple theoretical HFPs that essentially originate from the same radical structure. This mechanism was suggested in a previous study on α-L-rhamnose alkoxy radicals[59] and is currently under investigation for Fruc/R2.

5. Conclusion and Outlook

In the first part of this work, the effect of the molecular environment on first principles cluster in vacuo HFP calculations has been assessed in a series of sugar crystal radicals. This was done through a comparison with a reference set of HFPs calculated from periodic boundary simulations. It was shown that the cluster in vacuo models used in this study were able to reproduce the reference HFPs reasonably well in almost all cases, and all resulted in a good qualitative agreement with experimental data. In only a few cases, the cluster size was found to be too small to closely reproduce the reference isotropic HFPs. One example is the isotropic HFP of Fruc/R2/H3: although initial HFP calculations in a small cluster model resulted in a good agreement with one of the experimental values, additional calculations in an extended cluster model closely reproduced the reference result and, hence, proved that the earlier agreement was only coincidental.

A profound investigation of this residual discrepancy was performed by calculating the Fruc/R2/H3 isotropic HFP at every step along a Born−Oppenheimer molecular dynamics trajectory equilibrated at the experimental temperature using the hybrid AE + PSP GAPW scheme. Throughout this trajectory, the isotropic coupling fluctuated heavily, spanning a range of over 50 MHz, and comprised both reported experimental values. Although the average of these values did not bridge the gap between theoretical and experimental HFPs, the MD simulation did show that specific minor geometrical changes in the radical structure would bring the theoretical prediction much closer to the experimental HFPs. Although this study to some degree strengthened the validity of the proposed radical structure, several questions are still unanswered. One suggested phenom-

enon that could resolve the remaining problems assumes the existence of proton transfer along hydrogen bond chains across the entire crystal. This mechanism will be the subject of future work.

Acknowledgment. This work was supported by the Fund for Scientific Research−Flanders and the Research Board of Ghent University.

Supporting Information Available: Additional information as noted in text. This material is available free of charge via the Internet at http://pubs.acs.org.

References and Notes

(1) Debije, M. G.; Bernhard, W. A. *Radiat. Res.* **2001**, *155*, 687.
(2) Sagstuen, E.; Lund, A.; Awadelkarim, O.; Lindgren, M.; Westerling, J. *J. Phys. Chem.* **1986**, *90*, 5584.
(3) Vanhaelewyn, G.; Sadlo, J.; Callens, F.; Mondelaers, W.; De Frenne, D.; Matthys, P. *Appl. Radiat. Isot.* **2000**, *52*, 1221.
(4) Hohenberg, P.; Kohn, W. *Phys. Rev.* **1964**, *136*, B864.
(5) Kohn, W.; Sham, L. *Phys. Rev.* **1965**, *140*, A1133.
(6) Kaupp, M.; Bühl, M.; Malkin, V. G. *Calculations of NMR and EPR parameters: Theory and Applications*; Wiley-VCH: Weinheim, 2004.
(7) Pauwels, E.; Van Speybroeck, V.; Lahorte, P.; Waroquier, M. *J. Phys. Chem. A* **2001**, *105*, 8794.
(8) Pauwels, E.; Van Speybroeck, V.; Waroquier, M. *J. Phys. Chem. A* **2004**, *108*, 11321.
(9) Pauwels, E.; Van Speybroeck, V.; Waroquier, M. *Spectrochim. Acta, A* **2006**, *63*, 795.
(10) Blöchl, P. E. *Phys. Rev. B: Condens. Matter Mater. Phys.* **2000**, *62*, 6158.
(11) Van de Walle, C. G.; Blöchl, P. E. *Phys. Rev. B: Condens. Matter Mater. Phys.* **1993**, *47*, 4244.
(12) Csányi, G.; Arias, T. A. *Chem. Phys. Lett.* **2002**, *360*, 552.
(13) Yazyev, O. V.; Tavernelli, I.; Helm, L.; Röthlisberger, U. *Phys. Rev. B: Condens. Matter Mater. Phys.* **2005**, *71*, 115110.
(14) Bahramy, M. S.; Sluiter, M. H. F.; Kawazoe, Y. *Phys. Rev. B: Condens. Matter Mater. Phys.* **2006**, *73*, 045111.
(15) Declerck, R.; Pauwels, E.; Van Speybroeck, V.; Waroquier, M. *Phys. Rev. B: Condens. Matter Mater. Phys.* **2006**, *74*, 245103.
(16) Bühl, M.; Parrinello, M. *Chem.−Eur. J.* **2001**, *7*, 4487.
(17) Murakhtina, T.; Heuft, J.; Meijer, E. J.; Sebastiani, D. *Chem. Phys. Chem.* **2006**, *7*, 2578.
(18) Schmidt, J.; Sebastiani, D. *J. Chem. Phys.* **2005**, *123*, 074501.
(19) Blügel, S.; Akai, H.; Zeller, R.; Dederichs, P. H. *Phys. Rev. B: Condens. Matter Mater. Phys.* **1987**, *35*, 3271.
(20) Harriman, J. E. *Theoretical Foundations of Electron Spin Resonance*; Academic Press: New York, 1978.
(21) Granty, D. M.; Harris, K. M. *Encyclopedia of Nuclear Magnetic Resonance*; Wiley: Chicester, UK, 1996; Vol. 5.
(22) VandeVondele, J.; Krack, M.; Mohamed, F.; Parrinello, M.; Chassaing, T.; Hutter, J. *Comput. Phys. Commun.* **2005**, *167*, 103.
(23) http://cp2k.berlios.de (accessed June 1, 2007).
(24) Lippert, G.; Hutter, J.; Parrinello, M. *Theor. Chem. Acc.* **1999**, *103*, 124.
(25) Krack, M.; Parrinello, M. *Phys. Chem. Chem. Phys.* **2000**, *2*, 2105.
(26) Frisch, M. J.; Trucks, G. W.; Schlegel, H. B.; Scuseria, G. E.; Robb, M. A.; Cheeseman, J. R.; Montgomery, J. A., Jr.; Vreven, T.; Kudin, K. N.; Burant, J. C.; Millam, J. M.; Iyengar, S. S.; Tomasi, J.; Barone, V.; Mennucci, B.; Cossi, M.; Scalmani, G.; Rega, N.; Petersson, G. A.; Nakatsuji, H.; Hada, M.; Ehara, M.; Toyota, K.; Fukuda, R.; Hasegawa, J.; Ishida, M.; Nakajima, T.; Honda, Y.; Kitao, O.; Nakai, H.; Klene, M.; Li, X.; Knox, J. E.; Hratchian, H. P.; Cross, J. B.; Bakken, V.; Adamo, C.; Jaramillo, J.; Gomperts, R.; Stratmann, R. E.; Yazyev, O.; Austin, A. J.; Cammi, R.; Pomelli, C.; Ochterski, J. W.; Ayala, P. Y.; Morokuma, K.; Voth, G. A.; Salvador, P.; Dannenberg, J. J.; Zakrzewski, V. G.; Dapprich, S.; Daniels, A. D.; Strain, M. C.; Farkas, O.; Malick, D. K.; Rabuck, A. D.; Raghavachari, K.; Foresman, J. B.; Ortiz, J. V.; Cui, Q.; Baboul, A. G.; Clifford, S.; Cioslowski, J.; Stefanov, B. B.; Liu, G.; Liashenko, A.; Piskorz, P.; Komaromi, I.; Martin, R. L.; Fox, D. J.; Keith, T.; Al-Laham, M. A.; Peng, C. Y.; Nanayakkara, A.; Challacombe, M.; Gill, P. M. W.; Johnson, B.; Chen, W.; Wong, M. W.; Gonzalez, C.; Pople, J. A. *Gaussian 03*, Revision 05; gaussian, Inc.: Wallingford, CT, 2004.
(27) Madden, K. P.; Bernard, W. A. *J. Phys. Chem.* **1979**, *83*, 2643.
(28) Madden, K. P.; Bernard, W. A. *J. Phys. Chem.* **1982**, *86*, 4033.
(29) Vanhaelewyn, G. C. A. M.; Pauwels, E.; Callens, F. J.; Waroquier, M.; Sagstuen, E.; Matthys, P. F. A. E. *J. Phys. Chem. A* **2006**, *110*, 2147.
(30) Pauwels, E.; Van Speybroeck, V.; Vanhaelewyn, G.; Callens, F.; Waroquier, M. *Int. J. Quant. Chem.* **2004**, *99*, 102.
(31) Brown, G. M.; Levy, H. A. *Acta Crystallogr., B* **1979**, *35*, 656.
(32) Takagi, S.; Jeffrey, G. A. *Acta Crystallogr., B* **1997**, *33*, 3510.
(33) Becke, A. D. *Phys. Rev. A: At., Mol., Opt. Phys.* **1988**, *38*, 3098.
(34) Lee, C.; Yang, W.; Parr, R. G. *Phys. Rev. B: Condens. Matter Mater. Phys.* **1988**, *37*, 785.
(35) Godbout, N.; Salahub, D. R.; Andzelm, J.; Wimmer, E. *Can. J. Chem.* **1992**, *70*, 560.
(36) Lippert, G.; Hütter, J.; Ballone, P.; Parrinello, M. *J. Phys. Chem.* **1996**, *100*, 6231.
(37) Goedecker, S.; Teter, M.; Hutter, J. *Phys. Rev. B: Condens. Matter Mater. Phys.* **1996**, *54*, 1703.
(38) Hartwigsen, C.; Goedecker, S.; Hutter, J. *Phys. Rev. B: Condens. Matter Mater. Phys.* **1998**, *58*, 3641.
(39) Stewart, J. J. P. *J. Comp. Chem.* **1989**, *10*, 209.
(40) Stewart, J. J. P. *J. Comp. Chem.* **1989**, *10*, 221.
(41) Maseras, F.; Morokuma, K. *J. Comp. Chem.* **1995**, *16*, 1170.
(42) Svensson, M.; Humbel, S.; Froese, R. D. J.; Matsubara, T.; Sieber, S.; Morokuma, K. *J. Phys. Chem.* **1996**, *100*, 19357.
(43) Humbel, S.; Sieber, S.; Morokuma, K. *J. Chem. Phys.* **1996**, *105*, 1959.
(44) Matsubara, T.; Sieber, S.; Morokuma, K. *Int. J. Quantum Chem.* **1996**, *60*, 1101.
(45) Dapprich, S.; Komaromi, I.; Byun, K. S.; Morokuma, K.; Frisch, M. J. *J. Mol. Struct. (THEOCHEM)* **1999**, *461*, 1.
(46) Van, de Walle, C. G.; Blöchl, P. *Phys. Rev. B: Condens. Matter Mater. Phys.* **1993**, *47*, 4244.
(47) The isotropic HFPs of Gluc/R1/HO6, Gluc/R2/HO3, and Fruc/R1/HO3 were not taken up in this selection because their reference isotropic HFPs are too small (in absolute value) and disturb the relative fluctuations to an unrealistic extent.
(48) Barone, V.; Adamo, C.; Grand, A.; Subra, R. *Chem. Phys. Lett.* **1995**, *242*, 351.
(49) Barone, V.; Minichino, C.; Grand, A.; Subra, R. *J. Chem. Phys.* **1993**, *99*, 6787.
(50) Barone, V.; Grand, A.; Minichino, C.; Subra, R. *J. Phys. Chem.* **1993**, *97*, 6355.
(51) Martyna, G. J.; Klein, M. L.; Tuckerman, M. *J. Chem. Phys.* **1992**, *97*, 2635.
(52) Erling, P. A.; Nelson, W. H. *J. Phys. Chem. A* **2004**, *108*, 7591.
(53) Improta, R.; Barone, V. *Chem. Rev.* **2004**, *104*, 1231.
(54) Perdew, J. P.; Burke, K.; Ernzerhof, M. *Phys. Rev. Lett.* **1996**, *77*, 3865.
(55) Luchsinger, R. H.; Zhou, Y.; Meier, P. F. *Phys. Rev. B: Condens. Matter Mater. Phys.* **1997**, *55*, 6927.
(56) Porter, A. R.; Towler, M. D.; Needs, R. J. *Phys. Rev. B: Condens. Matter Mater. Phys.* **1999**, *60*, 13534.
(57) Marx, D.; Parrinello, M. *J. Chem. Phys.* **1996**, *104*, 4077.
(58) VandeVondele, J.; Mohamed, F.; Krack, M.; Hutter, J.; Sprik, M.; Parrinello, M. *J. Chem. Phys.* **2005**, *122*, 014515.
(59) Pauwels, E.; Declerck, R.; Van Speybroeck, V.; Waroquier, M. *Radiat. Res.*, in press.